We are IntechOpen, the world's leading publisher of Open Access books Built by scientists, for scientists

4,800
Open access books available

122,000
International authors and editors

135M
Downloads

Our authors are among the

154
Countries delivered to

TOP 1%
most cited scientists

12.2%
Contributors from top 500 universities

CLARIVATE ANALYTICS BOOK CITATION INDEX INDEXED

WEB OF SCIENCE™

Selection of our books indexed in the Book Citation Index in Web of Science™ Core Collection (BKCI)

Interested in publishing with us?
Contact book.department@intechopen.com

Numbers displayed above are based on latest data collected.
For more information visit www.intechopen.com

Chapter 11

Laser-Induced Fano Resonance in Condensed Matter Physics

Ken-ichi Hino, Yohei Watanabe,
Nobuya Maeshima and Muneaki Hase

Additional information is available at the end of the chapter

http://dx.doi.org/10.5772/intechopen.70524

Abstract

Recent development of laser technology toward the realization of high-power laser has opened up a new research area exploring various fascinating phenomena governed by strongly photoexcited electronic states in diverse fields of science. In this chapter, we review the laser-induced Fano resonance (FR) in condensed matter systems, which is one of the representative resonance effects successfully exposed by strong laser field. The FR of concern sharply differs from FR effects commonly observed in conventional quantum systems where FR is caused by a weak external perturbation in a stationary system in the following two aspects. One is that the present FR is a transient phenomenon caused by nonequilibrium photoexcited states. The other is that this is induced by an optically nonlinear process. Here, we introduce two physical processes causing such transient and optically nonlinear FR in condensed matter, followed by highlighting anomalous effects inherent in it. The first is a Floquet exciton realized in semiconductor superlattices driven by a strong continuous-wave laser, and the second is the coherent phonon induced by an ultrashort pulse laser in bulk crystals.

Keywords: laser, Fano resonance, photodressed states, exciton, dynamic localization, Floquet theorem, coherent phonon, ultrafast phenomena, polaronic quasiparticle

1. Introduction

In quantum systems where discrete levels are embedded in energetically degenerate continuum states, resonance phenomenon is likely manifested, that is, characteristic of asymmetric spectral profiles consisting of both a peak and a dip. This is known as Fano resonance (FR) [1]; this is also termed as either Feshbach resonance or many-channel resonance. FR is one of the

common and fundamental concepts in diverse fields of physics and chemistry; FR processes are observed, for instance, in strongly interacting Bose-Einstein condensates in an ultracold atomic system [2–4], superexcited states of molecules [5], a semiconductor quantum dot in an Aharonov-Bohm interferometer [6], an electronic transition near Weyl points strongly coupled with an infrared-active phonon in a Weyl semimetal [7].

In particular, within the restriction just to the FR processes triggered by laser irradiation, these may be classified in terms of the three categories as shown in **Table 1**. The first category is regarding whether a process is a linear one or a nonlinear one with respect to an order of a laser-matter interaction, as categorized as (a1) and (a2), respectively. For instance, the former is a photoabsorption process [8–11], and the latter is a multiphoton process [12–16]. The second category is regarding whether the process results from a built-in interaction between the discrete level and continuum that is intrinsic to a material itself or from a coupling induced extrinsically by a laser, as categorized as (b1) and (b2), respectively. For instance, the former is the interaction of an electron with a longitudinal optical (LO)-phonon in incoherent Raman scattering [17–22], and the electron-electron interaction brings about autoionization and the Auger process [23]. The latter FR process is known as a laser-induced continuum structure [2–4, 24]. The third category is regarding whether the process is a (quasi)stationary one or a transient one, as categorized as (c1) and (c2), respectively. In other words, this is whether (quasi)time-independent or time-dependent. For instance, the former is induced by a continuous-wave (cw) laser (monochromatic laser) [15, 16, 25, 26], and the latter is by a short pulsed laser [27–31].

It is stressed that for the FR categorized as (a2), its physical characters—such as asymmetry in spectral profile, spectral intensity, resonance position, and spectral width—are controllable in a quantum-mechanic manner by tuning various laser parameters. Thus, it is expected that underlying physics is enriched by intriguing effects inherent in this sort of FR. This differs from most of FR processes observed thus far because of being simply classified as (a1)-(b1)-(c1).

Currently, new research areas have been opened up owing to the progress of laser technology toward the realization of sophisticated high-power light sources. In particular, in the field of condensed matter physics, the development of high-intensity terahertz (THz) wave enables us to explore a photodressed quantum state in which a temporally periodic interaction of THz wave with matter is renormalized in the original quantum state in a nonperturbative manner [32–34]. Such an anomalous state is termed as a Floquet state because of ensuring the Floquet theorem [35]. Further, the development of ultrashort pulse laser—with its temporal width being of an

Category	**Characteristic**			
Optical process	(a1)	Linear (perturbative)	(a2)	Nonlinear (nonperturbative)
Interaction causing FR	(b1)	Intrinsic (built-in)	(b2)	Extrinsic (external)
Light source	(c1)	Monochromatic, continuous wave (stationary/quasistationary)	(c2)	Pulsed (transient)

Table 1. Classification of FR into three categories.

order of 10 femtosecond (fs)—enables us to explore ultrafast transitory phenomena governed by strongly photoexcited electronic states. Bearing in mind such current situations, here, we focus exclusively on the laser-induced FR effects realized in the following two physical systems. One is a Floquet exciton formed in semiconductor superlattices (SLs) driven by a strong THz wave, and the other is a coherent phonon (CP) generated by ultrashort pulse laser in bulk crystals. In the light of **Table 1**, the FR effects of concern sharply differ from those commonly observed in conventional quantum systems classified as (a1)-(b1)-(c1) in the following aspects. Both of the Floquet exciton and the CP are induced by optically nonlinear processes, and hence the significant quantum controls of FR are feasible by means of tuning the respective applied light sources. Further, the Floquet exciton forms manifolds of quasistationary states with quasienergy as a constant of motion, where the FR is mediated by the ac-Zener tunneling caused by the THz wave. Hence, this is classified as (a2)-(b2)-(c1) and is herein termed as dynamic FR (DFR). On the other hand, the CP is a transient phenomenon caused by the built-in interaction of an LO-phonon with nonequilibrium photoexcited carriers. Hence, this is classified as (a2)-(b1)-(c2) and is herein termed as transient FR (TFR).

Below, we survey the present research backgrounds of DFR and TFR in brief. In both cases, the applied electric field of pumping laser is represented as $F(t) = F_0(t)\cos(\omega t)$ with an envelope function $F_0(t)$ at time t and the center frequency ω.

To begin with the DFR, this is closely related with the photodressed miniband formation [36]. Here, the cw laser with a constant amplitude $F_0(t) \equiv F_{ac}$ gives rise to a nonlinear optical interaction with electron to result in a photodressed miniband with effective width $\Delta_{eff} = \Delta_0|J_0(x)|$, where Δ_0 and $J_0(x)$ represent the width of the original SL miniband and the zeroth-order Bessel function of the first kind with $x = eF_{ac}d/\hbar\omega$, respectively, and e, d, and $\hbar$ represent the elementary charge, a lattice constant of the SLs, and Planck's constant divided by 2π, respectively. Each photodressed miniband forms a sequence of photon sidebands arrayed at equidistant energy intervals of $\hbar\omega$ following the Floquet theorem. The DFR is caused by the interaction due to the ac-Zener tunneling between photon sidebands pertaining to different sequences, and this is coherently controlled by tuning F_{ac} and ω. In particular, it is expected that an anomalous effect attributed to dynamic localization (DL) on DFR is revealed on the occasion that all of the photodressed minibands collapse by tuning x to ensure $J_0(x) = 0$ [36–38]. The DL was first observed in electron-doped semiconductor SLs driven by a THz wave [39]. In addition, this has also been observed in diverse physical systems such as a cold atomic gas in one-dimensional optical lattices [40], a Bose-Einstein condensate [41], and light in curved waveguide arrays [42–44].

As regards the TFR, this was observed in a lightly n-doped Si crystal immediately after carriers were excited by an ultrashort laser pulse [45], where the speculation was made that the observed FR would show the evidence of the birth of a polaronic-quasiparticle (PQ) likely formed in a strongly interacting carrier-LO-phonon system in a moment [46]. The TFR of concern has been observed exclusively in this system and semimetals/metals such as Bi and Zn [47, 48] till now, however, not observed in p-doped Si and GaAs crystals [49, 50]. Thus far, there are a number of theoretical studies regarding these experimental findings. The time-dependent Schrödinger equation in the system of GaAs was calculated to show the asymmetric shape featuring FR

spectra, though apparently opposed to existing experimental results, as mentioned above [51]. Further, the classical Fano oscillator model was presented based on the Fano-Anderson Hamiltonian [52, 53], and the close comparison of the experimental results of the CP signals of Bi was made with the time signal obtained by taking the Fourier transform of Fano's spectral formula into a temporal region [48]. Recently, the authors have constructed a fully quantum-mechanical model based on the PQ picture in a unified manner on an equal footing between both of polar and nonpolar semiconductors such as undoped GaAs and undoped Si [31]. Here, it has been shown that the TFR is manifested in a flash only before the carrier relaxation time (∼100 fs) in undoped Si, whereas this is absent from GaAs.

Acronyms used in the text and the corresponding meanings are summarized in **Table 2**. The remainder of this chapter is organized as follows. In Section 2, the theoretical framework is described, where the models of the DFR and TFR are presented separately in Sections 2.1 and 2.2, respectively. The results and discussion are given in Section 3, and the conclusion with summary is given in Section 4. Atomic units (a.u.) are used throughout unless otherwise stated.

Acronyms	Meanings
CP	Coherent phonon
cw	Continuous wave
DFR	Dynamic FR
DL	Dynamic localization
FR	Fano resonance
fs	Femtosecond
LO	Longitudinal optical
PQ	Polaronic-quasiparticle
SL	Superlattice
TFR	Transient FR
THz	Terahertz

Table 2. Summary of acronyms used in text in alphabetical order and corresponding meanings.

2. Theoretical framework

2.1. Theoretical model for DFR in the photodressed exciton

2.1.1. Optical absorption spectra

The total Hamiltonian $\widehat{H}^{(DFR)}(t)$ concerned comprises a SL Hamiltonian consisting of field-free Hamiltonians of the conduction (c) and valence (v) bands, a Coulomb interaction between electrons, an intersubband interaction caused by the driving laser $F(t)$ polarized in the direction of crystal growth (the z-axis), and an interband interaction caused by the probe laser $f(t) = f_p \cos(\omega_p t)$ with the center frequency ω_p and the constant amplitude f_p; it is assumed that $F_{\mathrm{ac}} \gg f_p$ and

$\omega \ll \omega_p$. The microscopic polarization defined as $p_{\lambda\lambda'\boldsymbol{k}_\parallel}(t) \equiv \left\langle a^{(v)\dagger}_{\lambda\boldsymbol{k}_\parallel} a^{(c)}_{\lambda'\boldsymbol{k}_\parallel} \right\rangle$ is examined to shed light on the detail of DFR of the Floquet exciton; $\langle O \rangle$ represents the expectation value of the operator O. Here, $\lambda^{(\prime)} = (b^{(\prime)}, l^{(\prime)})$, which represents the lump of the SL miniband index $b^{(\prime)}$ and the SL site $l^{(\prime)}$. In addition, $\boldsymbol{k}_\parallel$ represents the in-plane momentum associated with the relative motion of the pair of c band and v band electrons, where the in-plane is defined as the plane normal to the z-axis; hereafter, the relative position conjugate to $\boldsymbol{k}_\parallel$ is represented as $\boldsymbol{\rho}$. Further, $a^{(s)\dagger}_{\lambda\boldsymbol{k}_\parallel}\left(a^{(s)}_{\lambda\boldsymbol{k}_\parallel}\right)$ represents the creation (annihilation) operator of the electron with λ and $\boldsymbol{k}_\parallel$ in band s.

The equation of motion for the microscopic polarization is given by the semiconductor Bloch equation

$$i\left(\frac{d}{dt} + \frac{1}{T_2}\right) p_{\lambda\lambda'\boldsymbol{k}_\parallel}(t) = \left\langle [a^{(v)\dagger}_{\lambda\boldsymbol{k}_\parallel} a^{(c)}_{\lambda\boldsymbol{k}_\parallel}, \widehat{H}^{(DFR)}(t)] \right\rangle \tag{1}$$

with T_2 dephasing time. For the practical purpose of tackling the multichannel scattering problem of exciton, it is convenient to transform it into the equation for $\overline{p}(\boldsymbol{\rho}, z_v, z_c, t)$ defined in the real-space representation as

$$\overline{p}(\boldsymbol{\rho}, z_v, z_c, t) = e^{i\omega_p t} \sum_{\lambda,\,\lambda'} \int d\boldsymbol{k}_\parallel e^{i\boldsymbol{k}_\parallel \cdot \boldsymbol{\rho}} \langle z_v|\lambda\rangle p_{\lambda\lambda'\boldsymbol{k}_\parallel}(t) \langle \lambda'|z_c\rangle, \tag{2}$$

where $\langle \lambda \,|\, z \rangle$ represents the Wannier function at position $z - ld$ in SL miniband b. The resulting equation becomes

$$\begin{aligned} &i\left(\frac{d}{dt} + \frac{1}{T_2} - i\omega_p\right)\overline{p}(\boldsymbol{\rho}, z_v, z_c, t) + (2\pi)^2 e^{i\omega_p t} f_0^{(+)}(t) d_0^{(vc)} \delta(\boldsymbol{\rho})\delta(z_v - z_c) \\ &= \int dz \left[\overline{p}(\boldsymbol{\rho}, z_v, z, t) H^{(c)}_{\mathrm{TB}}(z, z_c, t) - H^{(v)}_{\mathrm{TB}}(z_v, z, t)\overline{p}(\boldsymbol{\rho}, z, z_c, t)\right] + \mathcal{H}(\boldsymbol{\rho}, z_v, z_c)\overline{p}(\boldsymbol{\rho}, z_v, z_c, t), \end{aligned} \tag{3}$$

where the rotating wave approximation is employed by replacing $f(t)$ by $f_0^{(+)}(t) \equiv \left(f_p/2\right)e^{-i\omega_p t}$ and $d_0^{(vc)}$ represents the interband dipole moment of a bulk material. Here, the Hamiltonian $\mathcal{H}(\boldsymbol{\rho}, z_v, z_c)$ for the in-plane motion is given by $\mathcal{H}(\boldsymbol{\rho}, z_v, z_c) = -\nabla^2_{\boldsymbol{\rho}}/2m_\parallel + V(r)$, where $m_\parallel$ and $V(r) = -1/(\varepsilon_0 r)$ represent an in-plane reduced mass and the Coulomb interaction, respectively, with $r = \sqrt{\boldsymbol{\rho}^2 + (z_v - z_c)^2}$ and ε_0 the dielectricity of vacuum. The nearest-neighbor tight-binding Hamiltonian of the laser-driven SLs is given by $H^{(s)}_{\mathrm{TB}}(z, z', t) \equiv \left\langle z|\widehat{H}^{(s)}_{\mathrm{TB}}(t)|z'\right\rangle$, where

$$\widehat{H}^{(s)}_{\mathrm{TB}}(t) = \sum_{\lambda=(b,l)} \left[\varepsilon^{(s)}_{0b}|\lambda\rangle\langle\lambda| + \frac{(-1)^{b+\sigma^s}}{4}\Delta^{(s)}_b\left(|l,b\rangle\langle l+1,b| + |l+1,b\rangle\langle l,b|\right)\right] - F(t)\sum_{\lambda\lambda'}|\lambda\rangle Z^{(s)}_{\lambda\lambda'}\langle\lambda'|, \tag{4}$$

and $\varepsilon^{(s)}_{0b}$ and $\Delta^{(s)}_b$ represent the band center and the band width of b, respectively, with $\sigma^s = 0$ (for $s = c$) and 1 (for $s = v$). The last term of Eq. (4) represents the dipole interaction induced by the

driving laser $F(t)$ with $Z^{(s)}_{\lambda,\lambda'}$ as a dipole matrix element. It should be noted that the off-diagonal contribution of $Z^{(s)}_{\lambda,\lambda'}$ with $b \neq b'$ induces the ac-Zener tunneling, which plays a significant role of quantum control of DFR, as shown below.

The concerned function $\overline{p}(\boldsymbol{\rho}, z_v, z_c, t)$ can be expressed in terms of the complete set of the Floquet wave functions $\{\psi_{E\beta}(\boldsymbol{\rho}, z_v, z_c, t)\}$, that is,

$$\overline{p}(\boldsymbol{\rho}, z_v, z_c, t) = \int dE \sum_{\beta} a_{E\beta}\, \psi_{E\beta}(\boldsymbol{\rho}, z_v, z_c, t) \tag{5}$$

with $a_{E\beta}$ as an expansion coefficient. Here, the Floquet wave function ensures the following homogeneous equation associated with the inhomogeneous equation of Eq. (3) as

$$i\left(\frac{d}{dt} + E\right)\psi_{E\beta}(\boldsymbol{\rho}, z_v, z_c, t) = \int dz \left[\psi_{E\beta}(\boldsymbol{\rho}, z_v, z, t) H^{(c)}_{\mathrm{TB}}(z, z_c, t) - H^{(v)}_{\mathrm{TB}}(z_v, z, t)\psi_{E\beta}\boldsymbol{\rho}, z, z_c, t)\right]$$

$$+\mathcal{H}(\boldsymbol{\rho}, z_v, z_c)\psi_{E\beta}(\boldsymbol{\rho}, z_v, z_c, t), \tag{6}$$

where the temporally periodic boundary condition $\psi_{E\beta}(\boldsymbol{\rho}, z_v, z_c, t) = \psi_{E\beta}(\boldsymbol{\rho}, z_v, z_c, t+T)$ is imposed on it with E and $T = 2\pi/\omega$ as quasienergy and the time period of the driving laser field, respectively. Equation (6) is the Wannier equation of the Floquet exciton of concern. It should be noted that this is cast into the multichannel scattering equations and the Floquet state of $\psi_{E\beta}(\boldsymbol{\rho}, z_v, z_c, t)$ forms a continuum spectrum designated by both E and β with β representing the label of an open channel. Such a multichannel feature is introduced by the strong driving laser $F(t)$ that closely couples an excitonic-bound state with continua; more detail of the multichannel scattering problem is described in Section 2.1.2. The expansion coefficient $a_{E\beta}$ is readily obtained by inserting Eq. (5) into Eq. (3) in view of Eq. (6) as

$$a_{E\beta} = \frac{(2\pi)^2 d_0^{(vc)}\left(f_p/2\right)}{\left(E - \omega_p - i\gamma\right)T}\int_0^T dt' \overline{\psi}_{E\beta}(t'), \tag{7}$$

where $\overline{\psi}_{E\beta}(t) = \int dz \psi_{E\beta}(\mathbf{0}, z, z, t)$ and $\gamma = 1/T_2$.

Since the macroscopic polarization is given by $P(t) = \sum_{\lambda,\lambda'} \int d\boldsymbol{k}_{\parallel} d_0^{(vc)*} p_{\lambda\lambda'\boldsymbol{k}_{\parallel}}(t)$, the linear optical susceptibility $\chi(t)$ with respect to the weak probe laser $f(t)$ is cast into [54]

$$\chi(t) = \frac{\left|d_0^{(vc)}\right|^2}{\varepsilon_0}\int dE \sum_{\beta} \frac{O_{E\beta}(t)}{E - \omega_p - i\gamma}, \tag{8}$$

where $O_{E\beta}(t) = \left[\overline{\psi}_{E\beta}(t)/T\right]\int_0^T dt' \overline{\psi}^*_{E\beta}(t')$. Taking the Fourier transform of $\chi(t) \equiv \sum_j e^{ij\omega t}\chi_j(\omega_p; \omega)$, leads to the expression of the absorption coefficient to be calculated as

$$\alpha(\omega_p;\omega) = \frac{\omega_p}{C}\sum_j \mathrm{Im}\,\chi_j(\omega_p;\omega) \tag{9}$$

with C the speed of light; $\chi_{j\neq 0}(\omega_p;\omega)$ vanishes in the limit of $F_{ac}\to 0$.

2.1.2. Multichannel scattering problem

The absorption coefficient of Eq. (9) is obtained by evaluating a set of the wave functions, $\{\psi_{E\beta}(\boldsymbol{\rho}, z_v, z_c, t)\}$. To do this, first, the wave function is expanded as

$$\psi_{E\beta}(\boldsymbol{\rho}, z_v, z_c, t) = \sum_\mu \Phi_\mu(z_v, z_c, t) F_{\mu\beta}(\rho), \tag{10}$$

where $\rho = |\boldsymbol{\rho}|$, and just the contribution of the s-angular-momentum component is incorporated because of little effects from higher-order components. Here, $\Phi_\mu(z_v, z_c, t)$ is the real-space representation of the Floquet state $|\Phi_\mu\rangle$, that is, $\Phi_\mu(z_v, z_c, t) = \langle z_v, z_c | \Phi_\mu\rangle$, satisfying $\left(\widehat{H}_{\mathrm{TB}} - i\partial/\partial t\right)|\Phi_\mu\rangle = \mathcal{E}_\mu|\Phi_\beta\rangle$, where $\widehat{H}_{\mathrm{TB}} \equiv \widehat{H}^{(c)}_{\mathrm{TB}} + \widehat{H}^{(v)}_{\mathrm{TB}}$ and $\mathcal{E}_\mu$ is the μth quasienergy. The index μ is considered as the approximate quantum number $\mu \approx [\overline{\mu}, k]$ with $\overline{\mu} \equiv [b_c, b_v, n_p]$ as a photon sideband index, where b_c and b_v are SL miniband indexes belonging to the c- and v-bands, respectively, and k and n_p represent the Bloch momentum of the joint miniband of (b_c, b_v) and the number of photons relevant to absorption and emission, respectively. The quantum number $\overline{\mu}$ becomes a set of the good quantum numbers with F_{ac} decreasing, while k always remains conserved because of the spatial periodicity in the laser-driven SLs of concern. In view of Eq. (10), Eq. (6) is recast into the coupled equations for the radial wave function $F_{\nu\beta}(\rho)$, that is,

$$\sum_\mu L_{\mu\nu}F_{\nu\beta}(\rho) = EF_{\mu\beta}(\rho), \tag{11}$$

where $L_{\mu\nu}$ is an operator given by $L_{\mu\nu} = \delta_{\mu\nu}[-(2m_{\|})^1(d^2/d\rho^2 + \rho^1 d/d\rho) + \mathcal{E}_\mu] + V_{\mu\nu}(\rho)$ and $V_{\mu\nu}(\rho)$ is a Coulomb matrix element defined as $V_{\mu\nu}(\rho) = T^{-1}\int_0^T dt \int dz_v \int dz_c \Phi^*_\mu(z_v, z_c, t) V(\rho, z_v, z_c)$ $\Phi_\nu(z_v, z_c, t)$.

The Floquet exciton in the laser-driven SL system pertains to the multichannel scattering problem, because $V_{\mu\nu}(\rho)$ vanishes at $\rho \gg 1$. Actually, for a given E, the channel μ satisfying $E > \mathcal{E}_\mu$ is an open channel, while the channel μ satisfying $E < \mathcal{E}_\mu$ is a closed channel. Thus, the label μ of $F_{\mu\beta}$ plays the role of the scattering channel. On the other hand, the label β means the number of independent solutions satisfying Eq. (11). Here, there are same number of independent solutions as open channels, since as many scattering boundary conditions are imposed on $F_{\mu\beta}$ at $\rho \gg 1$; while evanescent boundary conditions that $F_{\mu\beta}$ vanishes at $\rho \gg 1$ are imposed on closed channels. Eq. (11) can be numerically evaluated by virtue of the R-matrix propagation method, which is a sophisticated formalism providing a stable numerical algorithm with extremely high accuracy [55].

It is expected that the DFR of concern is caused by a coupling between photon sidebands mediated by ac-Zener tunneling, as mentioned in Section 1. To see this situation in more detail,

Figure 1 shows the interacting two photon sidebands $\overline{\mu}$ and $\overline{\mu}' \equiv \left[b_c', b_v', n_p'\right]$, where the discrete Floquet excitonic state is supported by the photon sideband $\overline{\mu}$, and this is also embedded in the continuum of the alternative photon sideband $\overline{\mu}'$. It is likely that the DFR occurs due to a close coupling between these photon sidebands, and, eventually, the exciton state decays into the continuum state pertaining to $\overline{\mu}'$. In fact, it is noted that the Coulomb interaction incorporated in Eq. (6) also gives rise to FR. Defining the difference between the photon numbers of both photon sidebands, namely, $\Delta n_p = |n_p - n_p'|$, the ac-Zener tunneling is featured by $\Delta n_p \neq 0$, while the Coulomb coupling is by $\Delta n_p = 0$. The spectral profile and intensity of FR in the former can be even more effectively controlled than in the latter by modulating the laser parameters F_{ac} and ω, since the degree of magnitude of ac-Zener tunneling depends exclusively on both of the external parameters, differing from the Coulomb interaction. In the region of F_{ac} weak enough to suppress the ac-Zener tunneling, the FR is dominated by the Coulomb coupling, similarly to the conventional FR observed in the original SLs without laser irradiation [56].

2.2. Theoretical model for TFR in the CP generation

2.2.1. Introduction of polaronic quasiparticle operators

The total Hamiltonian $\widehat{H}^{(TFR)}$ of concern is given by $\widehat{H}^{(TFR)} = \widehat{H}_e + \widehat{H}'(t) + \widehat{H}_p + \widehat{H}_{e-p}$. Here, $\widehat{H}_e$ represents an electron Hamiltonian including an interelectronic Coulomb potential, where a two-band model is employed that consists of the energetically lowest c band and the energetically highest valence v band, and a creation (annihilation) operator of electron with band index b and Bloch momentum $\boldsymbol{k}$ is represented as $a_{b\boldsymbol{k}}^{\dagger}(a_{b\boldsymbol{k}})$. $\widehat{H}_p$ represents an LO-phonon

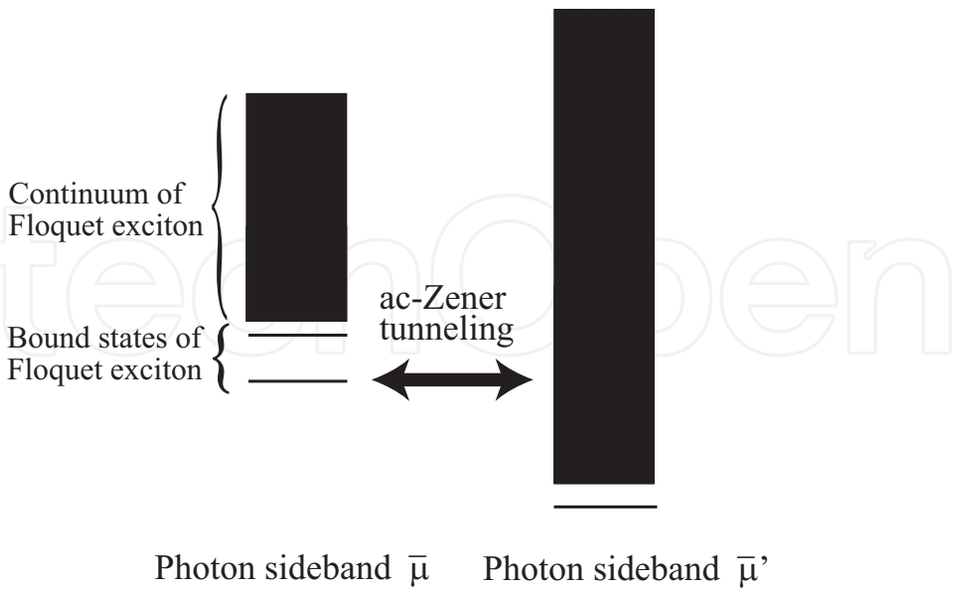

Figure 1. Schematic diagram of the DFR formation in the Floquet excitonic system. This shows the coupling mechanism that a bound state supported by the sideband $\overline{\mu}$ interacts with a continuum state belonging to the sideband $\overline{\mu}'$ by the ac-Zener tunneling to result in the Fano decay (from Ref. [15] with partial modification).

Hamiltonian, where a creation (annihilation) operator of LO-phonon with an energy dispersion $\omega_{\boldsymbol{q}}^{(LO)}$ at momentum $\boldsymbol{q}$ is represented as $c_{\boldsymbol{q}}^{\dagger}\left(c_{\boldsymbol{q}}\right)$. Further, $\widehat{H}'(t)$ and $\widehat{H}_{e-p}$ represent interaction Hamiltonians of electron with the pump pulse and the LO-phonon, respectively. These are given as follows:

$$\widehat{H}'(t) = -\frac{1}{2}\sum_{b,\, b'(\neq b),\, \boldsymbol{k}} \left[\Omega_{bb'}(t)\, a_{b\boldsymbol{k}}^{\dagger} a_{b'\boldsymbol{k}} + \Omega_{bb'}^{*}(t)\, a_{b'\boldsymbol{k}}^{\dagger} a_{b\boldsymbol{k}}\right], \tag{12}$$

where $\Omega_{bb'}(t) = d_{bb'}F(t)$ with $d_{bb'}$ an electric dipole moment between b and b' bands, and

$$\widehat{H}_{e-p} = \sum_{b,\, \boldsymbol{q},\, \boldsymbol{k}} \left(g_{b\boldsymbol{q}} c_{\boldsymbol{q}} a_{b\boldsymbol{k}+\boldsymbol{q}}^{\dagger} a_{b\boldsymbol{k}} + g_{b\boldsymbol{q}}^{*} c_{\boldsymbol{q}}^{\dagger} a_{b\boldsymbol{k}}^{\dagger} a_{b\boldsymbol{k}+\boldsymbol{q}}\right), \tag{13}$$

where $g_{b\boldsymbol{q}}$ is a coupling constant of b band electron with the LO-phonon. Here, let the envelope of $F(t)$ be of squared shape just for the sake of simplicity, that is, $F_0(t) = \mathcal{F}_0\theta(t+\tau_L/2)\theta(\tau_L/2-t)$ with $\mathcal{F}_0$ constant, where temporal width τ_L is of the order of a couple of 10 fs at most, satisfying $\tau_L \ll 2\pi/\omega_{\boldsymbol{q}}^{(LO)}$.

The equation of motion of a composite operator $A_{\boldsymbol{q}}^{\dagger}(\boldsymbol{k}bb') \equiv a_{b,\,\boldsymbol{k}+\boldsymbol{q}}^{\dagger} a_{b'\boldsymbol{k}}$ is considered below, where this represents an induced carrier density with spatial anisotropy determined by $\boldsymbol{q}$; $|\boldsymbol{q}|$ is finite, though quite small, that is, $\boldsymbol{q} \neq \boldsymbol{0}$. It is convenient to remove from this equation high-frequency contributions by means of the rotating-wave approximation [57] by replacing $A_{\boldsymbol{q}}^{\dagger}(\boldsymbol{k}bb')$ by $e^{i\overline{\omega}_{bb'}t}\overline{A}_{\boldsymbol{q}}^{\dagger}(\boldsymbol{k}bb')$, where $\overline{\omega}_{cv} = \omega$, $\overline{\omega}_{vc} = -\omega$, and $\overline{\omega}_{bb} = 0$. Thus, the resulting equation of motion is as follows:

$$\begin{aligned} -i\left(\frac{d}{dt} + \frac{1}{T_{\boldsymbol{q}}(\boldsymbol{k}bb')}\right)\overline{A}_{\boldsymbol{q}}^{\dagger}(\boldsymbol{k}bb') &= \left[\widehat{\mathcal{H}}_e(t), \overline{A}_{\boldsymbol{q}}^{\dagger}(\boldsymbol{k}bb')\right] - \overline{A}_{\boldsymbol{q}}^{\dagger}(\boldsymbol{k}bb')\overline{\omega}_{bb'} + \left[\widehat{H}_{e-p}, \overline{A}_{\boldsymbol{q}}^{\dagger}(\boldsymbol{k}bb')\right] \\ &\approx \sum_{\tilde{\boldsymbol{k}}\tilde{b}\tilde{b}'} \overline{A}_{\boldsymbol{q}}^{\dagger}\left(\tilde{\boldsymbol{k}}\tilde{b}\tilde{b}'\right)\overline{Z}_{\boldsymbol{q}}\left(\tilde{\boldsymbol{k}}\tilde{b}\tilde{b}', \boldsymbol{k}bb'\right) + \left[\widehat{H}_{e-p}, \overline{A}_{\boldsymbol{q}}^{\dagger}(\boldsymbol{k}bb')\right], \end{aligned} \tag{14}$$

where the total electronic Hamiltonian is defined as $\widehat{\mathcal{H}}_e(t) = \widehat{H}_e + \widehat{H}'(t)$, the first commutator in the right-hand side of the first equality is evaluated by making a factorization approximation, and $T_{\boldsymbol{q}}(\boldsymbol{k}bb')$ represents a phenomenological relaxation time constant relevant to $A_{\boldsymbol{q}}^{\dagger}(\boldsymbol{k}bb')$. Further, $\overline{Z}_{\boldsymbol{q}}$ represents a non-Hermitian matrix, which is a slowly varying function in time, since rapidly time-varying contributions are removed owing to the above rotating-wave approximation, aside from the discontinuity at $t = \pm\tau_L/2$.

Bearing in mind this situation, we tackle left and right eigenvalue problems of $\overline{Z}_{\boldsymbol{q}}$ [58], described by $U_{\boldsymbol{q}}^{L\dagger}\overline{Z}_{\boldsymbol{q}} = \mathcal{E}_{\boldsymbol{q}}U_{\boldsymbol{q}}^{L\dagger}$ and $\overline{Z}_{\boldsymbol{q}}U_{\boldsymbol{q}}^{R} = U_{\boldsymbol{q}}^{R}\mathcal{E}_{\boldsymbol{q}}$, respectively, in terms of an adiabatic-eigenvalue diagonal matrix $\mathcal{E}_{\boldsymbol{q}}$ and the associated biorthogonal set of adiabatic eigenvectors $\left\{U_{\boldsymbol{q}}^{L}, U_{\boldsymbol{q}}^{R}\right\}$ with time t fixed as a parameter. The orthogonality relation and the completeness

are read as $U_q^{L\dagger}U_q^R = 1$ and $U_q^R U_q^{L\dagger} = 1$, respectively [58]. Given the relation $\overline{Z}_q = U_q^R \mathcal{E}_q U_q^{L\dagger}$, Eq. (14) is recast into the form of adiabatic coupled equations:

$$-i\frac{dB_{q\alpha}^\dagger}{dt} = B_{q\alpha}^\dagger \mathcal{E}_{q\alpha} + i\sum_{\alpha'} B_{q\alpha'}^\dagger \mathcal{W}_{q\alpha'\alpha} + \left[\widehat{H}_{e-p}, B_{q\alpha}^\dagger\right], \tag{15}$$

where the operator $B_{q\alpha}^\dagger$ is defined as $B_{q\alpha}^\dagger \equiv \overline{A}_q^\dagger U_{q\alpha}^R$, $\mathcal{W}_{q\alpha'\alpha} \equiv \left[dU_{q\alpha'}^{L\dagger}/dt\right] U_{q\alpha}^R$, $+U_{q\alpha'}^{L\dagger} T_q^{-1} U_{q\alpha}^R$, and $\mathcal{E}_{q\alpha}(t)$ is complex adiabatic energy at time t associated with the operator $B_{q\alpha}^\dagger(t)$ thus introduced. Hereafter, this operator is termed as a creation operator of quasiboson, and the corresponding annihilation operator is defined as $B_{q\alpha} \equiv U_{q\alpha}^{R\dagger}\overline{A}_q$. The set of eigenstates $\{\alpha\}$ is composed of continuum states represented as β with eigenenergy $\mathcal{E}_{q\beta}$ and a single discrete energy state represented as α_1 with eigenenergy $\mathcal{E}_{q\alpha_1}$, that is, $\{\alpha\} = (\{\beta\}, \alpha_1)$; the state β corresponds to electron-hole continuum arising from interband transitions, and the state α_1 corresponds to a plasmon-like mode. It is noted that the relation of $\left\langle \left[B_{q\alpha}(t), B_{q'\alpha'}^\dagger(t)\right]\right\rangle = \delta_{qq'}\delta_{\alpha\alpha'}$ is assumed, though $B_{q\alpha}(t)$ and $B_{q\alpha}^\dagger(t)$ do not satisfy the equal-time commutation relations for a real boson, where $\widehat{X}$ means an expectation value of operator $\widehat{X}$ with respect to the ground state; the validity of the criterion of this relation is discussed in detail in Ref. [31].

Eq. (13) is rewritten as $\widehat{H}_{e-p} = \sum_{q,\alpha}\left(c_q B_{q\alpha}^\dagger M_{q\alpha} + M_{q\alpha}^* B_{q\alpha} c_q^\dagger\right)$ with an effective coupling between quasiboson and LO-phonon as $M_{q\alpha} = \sum_{kb} g_{bq} U_{q\alpha}^{L\dagger}(kbb)$. Thus, the commutator in Eq. (15) is approximately evaluated as $\left[\widehat{H}_{e-p}, B_{q\alpha}^\dagger\right] \approx M_{q\alpha}^{'*} c_q^\dagger$, though $M_{q\alpha}^{'*} \neq M_{q\alpha}^*$. On the other hand, the equation of motion of the LO-phonon is described by $-idc_q^\dagger/dt = \sum_\alpha B_{q\alpha}^\dagger M_{q\alpha} + c_q^\dagger \omega_q^{(LO)}$. Both of the equations of motion for $B_q^\dagger$ and $c_q^\dagger$ are integrated into a single equation in terms of matrix notations as follows:

$$-i\frac{d}{dt}\left(B_q^\dagger, c_q^\dagger\right) \approx \left(B_q^\dagger, c_q^\dagger\right) h_q + \left(iB_q^\dagger \mathcal{W}_q, 0\right). \tag{16}$$

Here, the non-Hermitian matrix $h_q \equiv \{h_{q\gamma\gamma'}\}$ given by $h_q = \begin{pmatrix} \mathcal{E}_q & M_q \\ M_q'^\dagger & \omega_q^{(LO)} \end{pmatrix}$ is introduced with $\gamma, \gamma' = 1 \sim N+2$, where N represents the number of electron-hole (discretized) continua, namely, $\beta = 1 \sim N$, aside from two discrete states attributed to a plasmon-like mode and an LO-phonon mode designated by α_1 and α_2, respectively: $\{\gamma\} = (\{\beta\}, \alpha_1, \alpha_2)$. In the system of the TFR of concern, the case is exclusively examined that both of the discrete levels of α_1 and α_2 are embedded into the continua $\{\beta\}$. Thus, the following coupled equations for the multichannel scattering problem are taken account of

$$\sum_{\gamma'} h_{q\gamma\gamma'} V_{q\gamma'\beta}^R = V_{q\gamma\beta}^R \mathcal{E}_{q\beta}, \tag{17}$$

where $V^R_{q\beta} = \left\{V^R_{q\gamma\beta}\right\}$ is the right vector representing the solution for given energy $\mathcal{E}_{q\beta}$; similarly to Eq. (11) for the DFR, the indices of γ and β play the roles of a scattering channel and the number of independent solutions, respectively. Eq. (17) provides the theoretical basis on which both of LO-phonon and plasmon-like modes are brought into connection with the CP dynamics on an equal footing. In terms of this vector, a set of N-independent operators, $F^\dagger_{q\beta}\ \left(\beta = 1 \sim N\right)$, is defined as

$$F^\dagger_{q\beta} = \sum_{\beta'} B^\dagger_{q\beta'} V^R_{q\beta'\beta} + B^\dagger_{q\alpha_1} V^R_{q\alpha_1\beta} + c^\dagger_q V^R_{q\alpha_2\beta}. \tag{18}$$

In addition, the left vector $V^{L\dagger}_{q\beta} = \left\{V^{L\dagger}_{q\beta\gamma}\right\}$ associated with $V^R_{q\beta}$ is introduced to ensure the inverse relations $B^\dagger_{q\alpha} = F^\dagger_q V^{L\dagger}_{q\alpha}$ and $c^\dagger_q = F^\dagger_q V^{L\dagger}_{q\alpha_2}$, where $V^{L\dagger}_q V^R_q = 1$ and $V^R_q V^{L\dagger}_q = 1$. Hereafter, the operator $F^\dagger_{q\beta}(t)$ thus introduced is termed as a creation operator of PQ, and then the corresponding annihilation operator is $F_{q\beta}(t)$; these are not bosonic operators. The bosonization scheme for the PQ operators is similar to that for the quasiboson operators, where the PQ ground state is given by the direct product of the ground states of quasiboson and LO-phonon and $\mathcal{E}_{q\beta}(t)$ is read as the single-PQ adiabatic energy at time t with mode $q\beta$.

Given Eq. (18), Eq. (16) becomes adiabatic coupled equations for $F^\dagger_q$:

$$-i\frac{d}{dt}F^\dagger_{q\beta} \approx F^\dagger_{q\beta}\mathcal{E}_{q\beta} + i\sum_{\beta'} F^\dagger_{q\beta'}\mathcal{I}_{q\beta'\beta}, \tag{19}$$

where $\mathcal{I}_q = \left(dV^{L\dagger}_q/dt\right)V^R_q + V^{L\dagger}_q \mathcal{W}_q V^R_q$. In terms of F_q and $F^\dagger_q$, the associated retarded Green function is given by [59]

$$G^R_{q\beta\beta'}(t,t') = -i\theta(t-t')\left\langle\left[F_{q\beta}(t), F^\dagger_{q\beta'}(t')\right]\right\rangle. \tag{20}$$

2.2.2. Transient induced photoemission spectra

A weak external potential $f_q(t)$ additionally introduced in the transient and nonequilibrium system of concern induces an electron density $n^{(ind)}_q(t)$ given by

$$n^{(ind)}_q(t) = \frac{1}{4\pi V}\int_{-\infty}^{t} dt' \chi^{(t)}_q(t,t') f_q(t'), \tag{21}$$

based on the linear response theory [59, 60] with V the volume of crystal. It is noted that $n^{(ind)}_q(t)$ is nonlinear with respect to the pump field. Here, $\chi^{(t)}_q(t,t')$ represents the retarded longitudinal susceptibility that depends on passage of t and the relative time $\tau = t - t'$, differing from equilibrium systems depending solely on τ. Introducing a retarded longitudinal

susceptibility due to the electron-induced interaction and that of an LO-phonon-induced interaction represented as $\chi_{\boldsymbol{q}}(t,t')$ and $\chi'_q(t,t')$, respectively, $\chi_{\boldsymbol{q}}^{(t)}(t,t')$ is given by [59]

$$\chi_{\boldsymbol{q}}^{(t)}(t,t') = \chi_{\boldsymbol{q}}(t,t') + \chi'_{\boldsymbol{q}}(t,t'). \tag{22}$$

Let $f_{\boldsymbol{q}}(t')$ be assumed to be $f_{\boldsymbol{q}}(t') = f_{\boldsymbol{q}0}\,\delta(t'-t_p)$ in the present system; $f_{\boldsymbol{q}0}$ is independent of t', and t_p represents the time at which $f_{\boldsymbol{q}}(t')$ probes transient dynamics of concern. Thus, it is seen that $\chi_{\boldsymbol{q}}^{(t)}(t,t_p)$ reveals the way of alteration of $n_{\boldsymbol{q}}^{(ind)}(t)$ after t_p, since Eq. (21) becomes $n_{\boldsymbol{q}}^{(ind)}(t) = f_{\boldsymbol{q}0}\chi_{\boldsymbol{q}}^{(t)}(t,t_p)\theta(t-t_p)/4\pi V$.

In terms of $\chi_{\boldsymbol{q}}^{(t)}(t_p+\tau,t_p)$, the dielectric function $\varepsilon_{\boldsymbol{q}}(t_p+\tau,t_p)$ is readily obtained, and by taking the Fourier transform of it as $\tilde{\varepsilon}_{\boldsymbol{q}}(t_p;\omega_p) = \int_0^\infty d\tau\, e^{-i\omega_p\tau}\varepsilon_{\boldsymbol{q}}(t_p+\tau,t_p)$, this leads to a transient absorption coefficient $\alpha_{\boldsymbol{q}}(t_p;\omega_p)$ at time t_p. This is given by $\alpha_{\boldsymbol{q}}(t_p;\omega_p) = \omega A_{\boldsymbol{q}}(t_p;\omega_p)/n(t_p;\omega_p)C$, where $A_{\boldsymbol{q}}(t_p;\omega_p) = \mathrm{Im}\,\tilde{\varepsilon}_{\boldsymbol{q}}(t_p;\omega_p)$ and $n(t_p;\omega_p)$ represents the index of refraction. It is remarked that according to the definition of the sign of ω_p made above, transient photoemission spectra, where $A_{\boldsymbol{q}}(t_p;\omega_p)<0$, peak at positive ω_p, while transient photoabsorption spectra, where $A_{\boldsymbol{q}}(t_p;\omega_p)>0$, peak at negative ω_p. For the sake of the later convenience, the transient induced photoemission spectra are defined as $\overline{A}_{\boldsymbol{q}}(t_p;\omega_p) = -A_{\boldsymbol{q}}(t_p;\omega_p)$.

Based on the PQ model developed in Section 2.2.1, $\chi_{\boldsymbol{q}}(t,t')$ and $\chi'_{\boldsymbol{q}}(t,t')$ can be explicitly expressed in terms of the retarded Green function given by Eq. (20). Here, the obtained results are shown below; for more detail, consult Ref. [31]:

$$\chi^*_{\boldsymbol{q}}(t,t') = \frac{4\pi}{V}\sum_{\alpha\alpha'\beta\beta'} N^{L*}_{\boldsymbol{q}\alpha}(t)V^{L}_{\boldsymbol{q}\alpha\beta}(t)G^{R}_{\boldsymbol{q}\beta\beta'}(t,t')V^{L\dagger}_{\boldsymbol{q}\beta'\alpha'}(t')N^{L}_{\boldsymbol{q}\alpha'}(t'), \tag{23}$$

where $N^L_{\boldsymbol{q}\alpha} = \sum_{\boldsymbol{k}b} U^{L\dagger}_{\boldsymbol{q}\alpha}(\boldsymbol{k}bb)$, and this is equivalent to a normalization constant of the left vector $U^{L\dagger}_{\boldsymbol{q}\alpha}$:

$$\chi'_{\boldsymbol{q}}(t,t') = \frac{4\pi}{V}\left|g'_{\boldsymbol{q}}\right|^2\left[\overline{D}'^{R}_{\boldsymbol{q}}(t,t') + \left[\overline{D}'^{R}_{-\boldsymbol{q}}(t,t')\right]^*\right], \tag{24}$$

where $g'_{\boldsymbol{q}}$ is a constant in proportion to $(g_{c\boldsymbol{q}}+g_{v\boldsymbol{q}})/2$ and

$$\overline{D}'^{R}_{\boldsymbol{q}}(t,t') = \sum_{\beta\beta'} V^{L}_{\boldsymbol{q}\alpha_2\beta}(t)G^{R}_{\boldsymbol{q}\beta\beta'}(t,t')V^{L\dagger}_{\boldsymbol{q}\beta'\alpha_2}(t'). \tag{25}$$

Finally, the TFR dynamics caused by the CP generation is mentioned based on the PQ picture. As shown in **Figure 2**, the LO-phonon state α_2 is embedded in the quasiboson state β, and the effective coupling between both states induces the formation of transient PQ FR state. This composite state is deexcited into the PQ ground state via two paths: one is the transient photoemission from α_2, and the other is from β. It is likely that these two paths interfere to

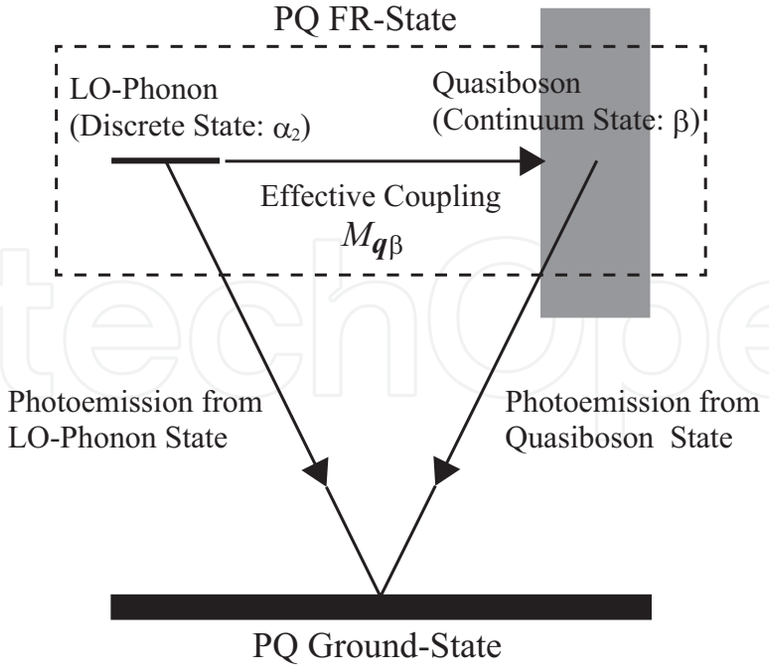

Figure 2. Schematic diagram of the TFR dynamics based on the PQ picture, where the LO-phonon state α_2 is embedded in the quasiboson state β. The PQ FR state composed of α_2 and β is deexcited by induced photoemission process. For more detail, consult the text (from Ref. [31] with partial modification).

give rise to asymmetry in spectra. It is remarked that the contribution from the plasmon-like mode α_1 is omitted because of a negligibly smaller effect on the TFR.

3. Results and discussion

3.1. DFR in the photodressed exciton

For the calculations of DFR spectra, the semiconductor SLs of GaAs/$Ga_{0.75}Al_{0.25}As$ are employed with 35/11 monolayers (ML) for the well and barrier thickness, where 1 ML = 2.83 Å. Here, 14 photon sidebands of $\overline{\mu} = [1, 1, -3 \sim 3]$ and $[2,1,-3\sim3]$ are incorporated by setting ω to 91 meV; this equals to the difference between the centers of the joint minibands of (1,1) and (2,1). Other photon sidebands are neglected for the sake of simplicity.

First of all, the calculated quasienergy bands $\{\mathcal{E}_\mu\}$ as a function of F_{ac} are shown in **Figure 3** to illustrate the effect of ac-Zener coupling. The two photon sidebands labeled by $\mu_1 = [1,1,0,k]$ and $\mu_2 = [2,1,-1,k]$ are mixed by the coupling induced by the driving laser $F(t)$. With the increase of F_{ac}, the quasienergy bands are branched into two distinct photon sidebands, termed as the upper sideband μ_+ and the lower sideband μ_-, where both labels of μ_1 and μ_2 are no longer good quantum numbers, aside from k. It is noted that both of μ_+ and μ_- form dynamic localization showing band collapse around two points $F_{ac} = F_{DL1} \equiv 170$ kV/cm and $F_{DL2} \equiv 395$ kV/cm. **Figure 4** shows the absorption spectra $\alpha(\omega_p;\omega)$ obtained by solving Eq. (9) in the range of F_{ac} from 10 to 450 kV/cm. Asymmetric spectral profiles characteristic of DFR are discerned at the arrowed positions of ω_p when $F_{ac} \geq 150$ kV/cm, where all peaks are followed by dips. These

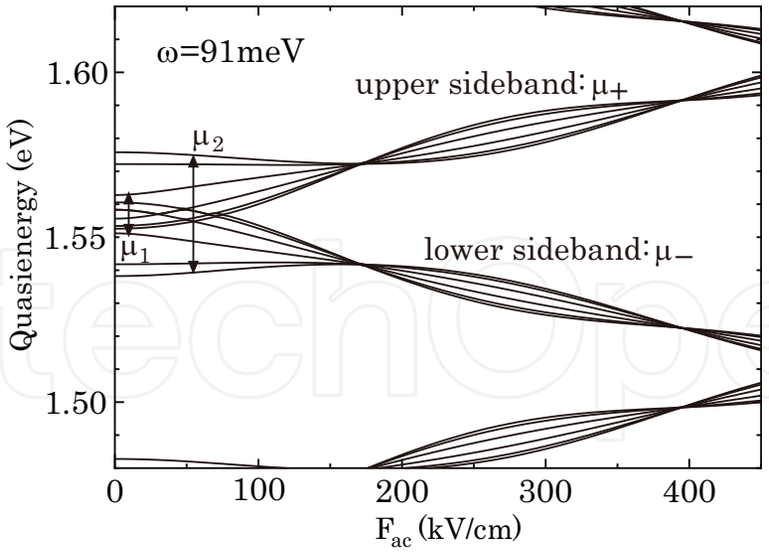

Figure 3. The quasienergy $\mathscr{E}_\mu$ as a function of F_{ac}. ω is set to 91 meV. The vertical double arrows represent the original SL miniband widths corresponding to the photon sidebands of μ_1 and μ_2 (from Ref. [16] with partial modification).

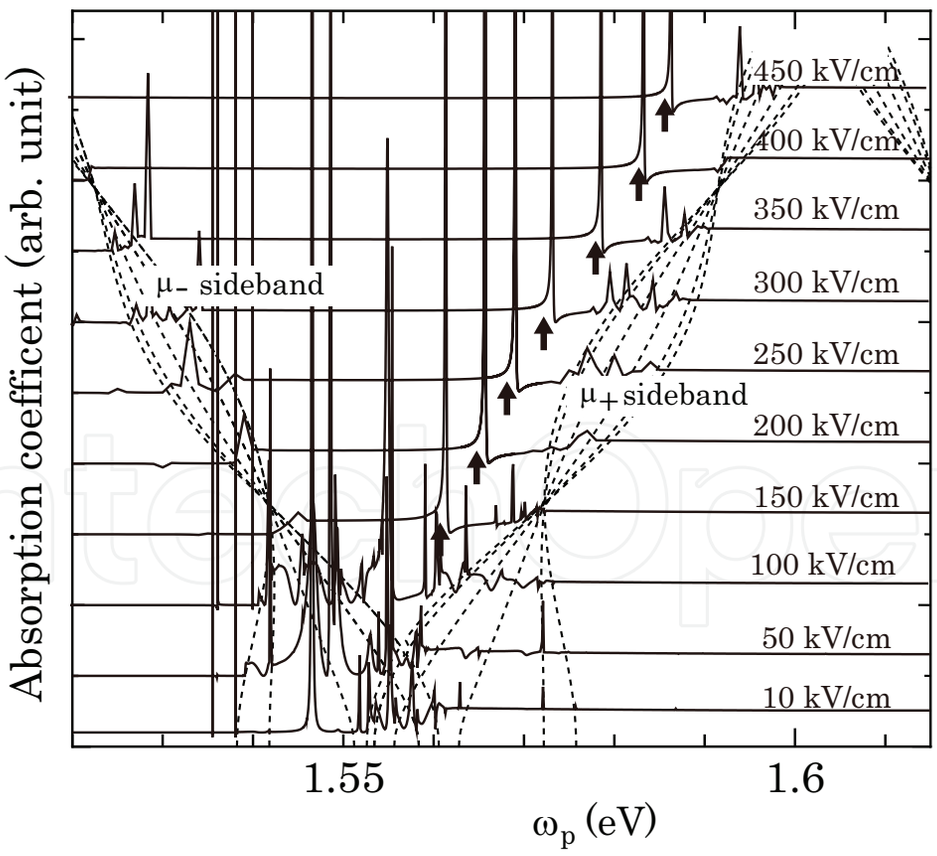

Figure 4. Absorption spectra $\alpha(\omega_p;\omega)$ as a function of ω_p for F_{ac}=50–450 (kV/cm) with ω= 91 meV. A series of the arrowed spectral profiles are examined exclusively in the text. The quasienergies shown in **Figure 3** are also plotted (dotted lines) (from Ref. [16] with partial modification).

peaks are located just below the upper sideband μ_+, thereby being blue shifted. Consulting **Figure 1**, the DFR is dominantly formed by the interaction between one open channel μ_- and one closed channel μ_+.

To deepen the understanding of the DFR exciton, its characteristic quantities determining the spectral profiles are extracted from $\alpha(\varepsilon) \equiv \alpha(\omega_p;\omega)$ arrowed in **Figure 4** by being fitted to Fano's Formula [1]:

$$\alpha(\varepsilon) = \alpha_0 \frac{\left(\varepsilon + q^{(F)}\right)^2}{\varepsilon^2 + 1}, \tag{26}$$

in the vicinity of an excitonic resonance quasienergy $\mathcal{E}_{ex}$, where $\varepsilon = 2(\omega_p - \mathcal{E}_{ex})/\Gamma$ with the spectral width Γ and the asymmetry parameter (Fano's q-parameter) $q^{(F)}<0$. **Figure 5(a)** shows the evaluated values of $|1/q^{(F)}|$ and Γ as a function of F_{ac}, while **Figure 5(b)** shows the peak intensity $\alpha(0) = \alpha_0[q^{(F)}]^2 \equiv \alpha_{max}$ and background spectra $\alpha(\pm\infty) = \alpha_0$ as a function of F_{ac}. It is seen that these functions are affected pronouncedly by F_{ac}; in particular, extrema are formed around $F_{ac} = F_{DL1}$. It is remarked that with the decrease in $|1/q^{(F)}|$ and Γ, the DFR state becomes a pure bound state. In addition, there still exist faint extrema around $F_{ac} = F_{DL2}$ in the concerned quantities except Γ. Therefore, the DL is considered to fulfill a special role of the quantum control of photodressed excitonic states.

For the purpose of confirming such an effect of DL and the pronounced F_{ac} dependence of related quantities on the excitonic DFR, one evaluates the transition probability between the photon sidebands of μ_1 and μ_2 due to the ac-Zener coupling; this value is represented as $M(F_{ac})$ as a function of F_{ac}. This corresponds to the degree of mixing between these two photon

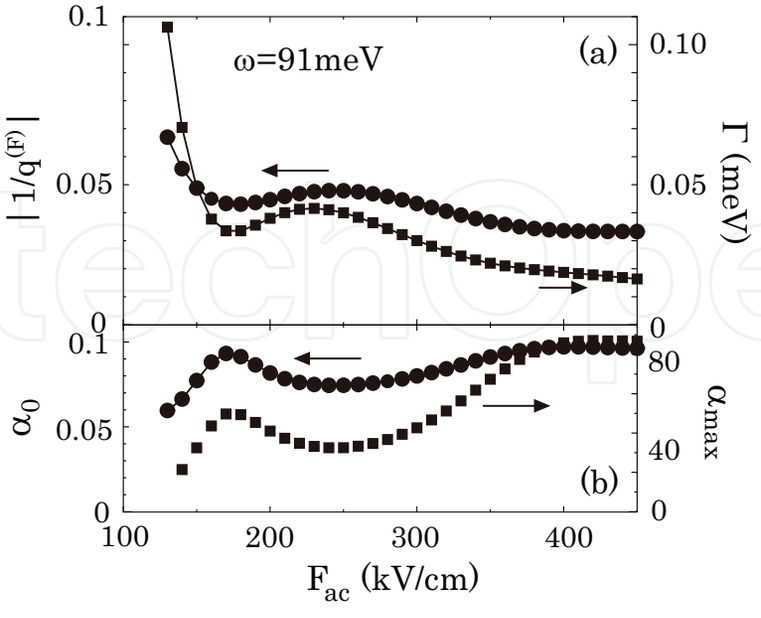

Figure 5. The DFR-related quantities as a function of F_{ac} with the fixed value of ω=91 meV. The calculated results represented by the filled symbols are connected by the solid lines in order to aid the presentation. (a) $|1/q^{(F)}|$ and Γ and (b) α_0 and α_{max} (from Ref. [16] with partial modification).

sidebands. $M(F_{ac})$ is readily obtained by solving the associated coupled equations between μ_1 and μ_2 in an approximate manner of neglecting contributions from all other photon sidebands [16]. Given $\Delta\varepsilon$ and v as the difference of ac-Zener-free quasienergies between μ_1 and μ_2, and the matrix element of the ac-Zener coupling between them, respectively, $M(F_{ac})$ is provided as

$$M(F_{ac}) = \left[\sin\left(\phi/2\right)\right]^2 = \frac{1}{2}\left(1 - \frac{1}{\sqrt{1+z^2}}\right), \tag{27}$$

where $z \equiv \tan\phi = 2|v|/|\Delta\varepsilon|$. With $x = F_{ac}d/\omega$, v and $\Delta\varepsilon$ are evaluated as $v \propto x$ and $\Delta\varepsilon \propto \cos(kd)J_0(x)$, respectively; see Section 1. Thus, one has $z = 2x/\eta J_0(x)$ where η is a proportional constant between $\Delta\varepsilon$ and v. According to Eq. (27), for finite values of η, with the increase of F_{ac}, $M(F_{ac})$ increases from 0 to 1/2 in an oscillating manner; for more detail of the shape of $M(F_{ac})$ for several values of η, consult Ref. [16].

The alteration pattern of $M(F_{ac})$ with respect to F_{ac} looks somewhat similar to the shapes of the DFR-related functions shown in **Figure 5**. In particular, it is noted that $M(F_{ac})$ has extrema at zeros of $J_0(x)$, which just correspond to DL concerned here; that is, $M(F_{ac})$ shows extrema at $F_{ac} = F_{DL1}$ and F_{DL2}. In fact, $M(F_{ac})$ shows a clear extremum at $F_{ac} = F_{DL1}$, while the second extremum at $F_{ac} = F_{DL2}$ is not obviously discernible. This is understood by the behavior that the oscillating component incorporated in $J_0(x)$ is overwhelmed by the ac-Zener coupling v for large x. Therefore, it is concluded that the characteristic F_{ac} dependence of the functions of $|1/q^{(F)}|$, Γ, $\alpha_{\max}$, and α_0 is attributed to the competition between the ac-Zener effect and the band width of the free electron-hole pair states in the vicinity of the DL positions.

Finally, one mentions in brief the ω dependence of the physical quantities $|1/q^{(F)}|$ and Γ at F_{ac}=180 kV/cm in the vicinity of $F_{ac} = F_{DL1}$. As shown in **Figure 6(a)**, $|1/q^{(F)}|$ decreases sharply with the increase in ω, while Γ is maximized around ω = 91 meV at which the centers of two photon sidebands μ_1 and μ_2 coincide. The tendency of $|1/q^{(F)}|$ is in harmony with the ω dependence of the ratio of d_c to d_o, namely, $r_d = d_c/d_o$, as shown in **Figure 6(b)**, where d_c and d_o represent a dipole-transition matrix from the ground state to the closed channel μ_+ and that to the open channel μ_-, respectively. Actually, r_d is in proportion to $q^{(F)}$ [16]. Such alteration of r_d is interpreted on the basis of the anticrossing formation of photon sidebands of μ_+ and μ_- due to the Autler-Townes effect, though not discussed here; for more detail, consult Ref. [16]. Thus, it seems that comparing **Figure 6(a)** with **Figure 5(a)**, the q parameter is even more controllable by changing ω than by F_{ac}.

3.2. TFR in the CP generation

For the calculations of TFR spectra of undoped Si and undoped GaAs, the associated materials parameters employed in the present study are shown in Ref. [31], while parameters of a square-shaped pulse laser employed are as follows. For undoped Si and undoped GaAs, detuning with reference to energy band gap $\Delta\omega$=82 and 73 meV, respectively, temporal width τ_L=15 fs, pulse area A_L=0.12π and 0.20π, respectively, and the maximum excited electron density N_{ex}^0=6.31×10^{17} and $5.30\times10^{17}\,\mathrm{cm}^3$, respectively; by $\Delta\omega$>0, it is meant that opaque interband transitions with real excited carriers are examined. Further, two time constants of

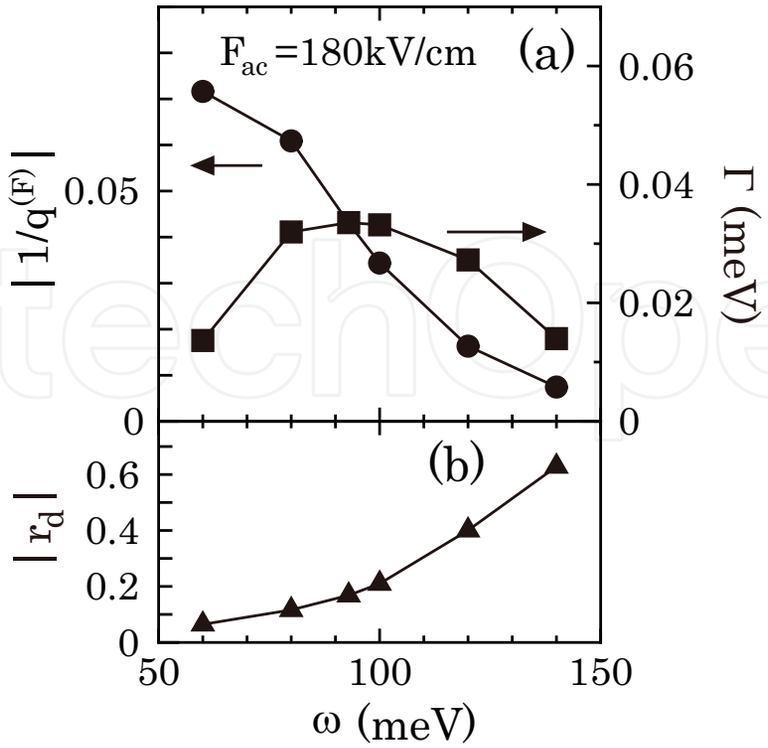

Figure 6. The DFR-related quantities as a function of ω with the fixed value of F_{ac}=180 meV. The calculated results represented by the filled symbols are connected by the solid lines in order to aid the presentation. (a) $|1/q^{(F)}|$ and Γ and (b) $|r_d|$ (from Ref. [16] with partial modification).

T_{12} and $T_{\boldsymbol{q}12}$ are introduced, which represent phenomenological damping time constants of induced carrier density with isotropic momentum distribution and anisotropic momentum distribution with $\boldsymbol{q}$, respectively. The temporal region $t<T_{12}$ is termed as the early-time region during which a great number of carriers still stay in excited states, and the quantum processes govern the CP dynamics; $T_{\boldsymbol{q}12}$ is approximately equal to $T_{\boldsymbol{q}}(\boldsymbol{k}bb')$ introduced in Eq. (14). On the other hand, the temporal region $t \gtrsim T_{12}$ is termed as the classical region. For the present calculations, $T_{\boldsymbol{q}12}$ and T_{12} are set equal to 20 and 90 fs, respectively. As regards experimental estimates of these time constants for Si, $T_{\boldsymbol{q}12}$ and T_{12} extracted from the CP measurements in Ref. [45] are 16 and 100 fs, respectively, at $N_{ex}^0 = 4 \times 10^{19}\,\mathrm{cm}^{-3}$.

Transient induced photoemission spectra $\overline{A}_{\boldsymbol{q}}(t_p, \omega_p)$ defined in Section 2.2.2 show the change of excited electronic structure due to the pump field at probe time t_p, and this is crucial to understand the TFR accompanied by CP generation. The total retarded longitudinal susceptibility consists of the dynamically screened Coulomb interaction induced by electron and the LO-phonon-induced interaction. That is, $\tilde{\chi}_{\boldsymbol{q}}^{(t)}(t_p;\omega_p) = \tilde{\chi}_{\boldsymbol{q}}(t_p;\omega_p) + \tilde{\chi}_{\boldsymbol{q}}'(t_p;\omega_p)$, where this is a Fourier transform of Eq. (22) with respect to τ into the ω_p domain. In the small transferred momentum $\boldsymbol{q}$ limit, $\tilde{\chi}_{\boldsymbol{q}}(t_p;\omega_p)$ is proportional to $|\boldsymbol{q}|^2$, while $\tilde{\chi}_{\boldsymbol{q}}'(t_p;\omega_p)$ is proportional to $|\boldsymbol{q}|^2$ for the Fröhlich interaction exclusively for a polar crystal such as GaAs and to $|\boldsymbol{q}|^4$ for the deformation potential interaction. This difference is attributed to the fact that the Fröhlich interaction is of long range, and the deformation potential interaction is of short range. It is

noted that in a nonpolar crystal such as Si, a dipole transition for lattice absorption vanishes in the limit of $\boldsymbol{q} = \mathbf{0}$ because of the presence of spatial inversion symmetry [61].

In **Figures 7** and **8**, $\overline{A}_{\boldsymbol{q}}(t_p;\omega_p)$ of Si and GaAs as a function of ω_p is shown, respectively, by solid lines at t_p equal to $t_1 \equiv 15$, $t_2 \equiv 65$ and $t_3 \equiv 100$ fs, where the separate contributions from $\tilde{\chi}_{\boldsymbol{q}}(t_p;\omega_p)$ and $\tilde{\chi}'_{\boldsymbol{q}}(t_p;\omega_p)$ are also shown by chain and dashed lines, respectively. $\tilde{\chi}_{\boldsymbol{q}}(t_p;\omega_p)$ and $\tilde{\chi}'_{\boldsymbol{q}}(t_p;\omega_p)$ are mostly governed by the plasmon-like mode α_1 and the LO-phonon mode α_2, respectively. In both figures, it is seen that just $\tilde{\chi}'_{\boldsymbol{q}}(t_p;\omega_p)$ contributes to the formation of spectral peaks and becomes dominant over $\tilde{\chi}_{\boldsymbol{q}}(t_p;\omega_p)$ in the classical region.

Figure 7(a) shows $\overline{A}_{\boldsymbol{q}}(t_p;\omega_p)$ of Si at $t_p = t_1 < T_{\mathbf{q}12}$, where the obtained continuum spectra are governed by the contribution from $\tilde{\chi}_{\boldsymbol{q}}(t_p;\omega_p)$, whereas the contribution from $\tilde{\chi}'_{\boldsymbol{q}}(t_p;\omega_p)$ is negligibly small due to the proportion of it to $|\boldsymbol{q}|^4$. In Figure 7(b) at $t_p = t_2$ with $T_{\boldsymbol{q}12} < t_p < T_{12}$, the contributions from $\tilde{\chi}_{\boldsymbol{q}}(t_p;\omega_p)$ are damped to be comparable to those from $\tilde{\chi}'_{\boldsymbol{q}}(t_p;\omega_p)$. It is noted that asymmetric spectra characteristic of FR are manifested with a dip followed by a peak. This is in sharp contrast with a symmetric Lorentzian profile shown in **Figure 7(c)** at $t_p = t_3 > T_{12}$. As regards $\overline{A}_{\boldsymbol{q}}(t_p;\omega_p)$ of GaAs, it is shown in **Figure 8(a)** that at $t_p = t_1$, a pronounced peak due to the α_2 mode, is superimposed with a continuum background composed of $\tilde{\chi}_{\boldsymbol{q}}(t_p;\omega_p)$ and $\tilde{\chi}'_{\boldsymbol{q}}(t_p;\omega_p)$ with comparable order, since both are in proportion to $|\boldsymbol{q}|^2$. The spectra at $t_p = t_2$ shown in **Figure 8(b)** are dominated by $\tilde{\chi}'_{\boldsymbol{q}}(t_p;\omega_p)$, differing a lot from those shown in **Figure 7(b)** of Si. The spectra at $t_p = t_3$ in **Figure 8(c)** are similar to those in **Figure 7(c)**.

The origin of the manifestation of TFR in Si shown in **Figure 7(b)** is examined below. The principal difference between Si and GaAs observed here is attributed just to the effective coupling $M_{\boldsymbol{q}\beta}$ between quasiboson and LO-phonon aside from less significant difference in other material parameters; this appears in the matrix $h_{\boldsymbol{q}}$ introduced in Eq. (16), and the approximation of $M_{\boldsymbol{q}} \approx M'_{\boldsymbol{q}}$ is employed here. The primitive coupling constant $g_{b\mathbf{q}}$ incorporated in $M_{\boldsymbol{q}\beta}$ consists of $g^D_{b\boldsymbol{q}}$ and $g^F_{b\boldsymbol{q}}$ representing the coupling constants due to a phenomenological

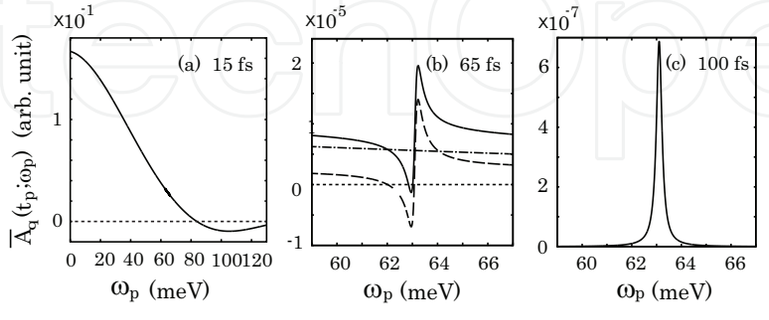

Figure 7. $\overline{A}_{\boldsymbol{q}}(t_p,\omega_p)$ of undoped Si (solid line) as a function of ω_p at t_p equal to (a) 15 fs, (b) 65 fs, and (c) 100 fs. Separate contributions to the spectra from $\tilde{\chi}_{\boldsymbol{q}}(t_p;\omega_p)$ and $\tilde{\chi}'_{\boldsymbol{q}}(t_p;\omega_p)$ are also shown by chain and dashed lines, respectively. $\overline{A}_{\boldsymbol{q}}(t_p;\omega)$ is reckoned from structureless background due to electron-hole continuum states β that are almost constant in the ω_p region concerned. The widths of the spectral peaks are determined by a phenomenological damping constant T_{ph} of LO-phonon due to lattice anharmonicity: $2/T_{ph}$=0.27 meV (from Ref. [31] with partial modification).

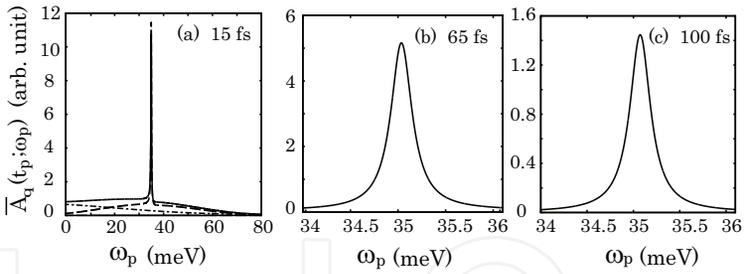

Figure 8. The same as **Figure 7** but for undoped GaAs (from Ref. [31] with partial modification).

LO-phonon deformation potential interaction and the Fröhlich interaction, respectively, that is, $g_{bq} = g^D_{bq} + g^F_{bq}$. Here, g^D_{bq} is real and approximately independent of q, while g^F_{bq} is pure imaginary and $|g^F_{bq}| \propto |q|^{-1}$ [61]. In a nonpolar crystal such as Si, $g_{bq} = g^D_{bq}$, whereas in a polar or partially ionic crystal such as GaAs, g^F_{bq} is much dominant to g^D_{bq}, namely, $g_{bq} \approx g^F_{bq}$. Actually, the phase of $M_{q\beta}$ is almost determined by that of g_{bq}, since a residual factor defining $M_{q\beta}$ is almost considered real. Thus, $M_{q\beta}$ is a complex number given by $M_{q\beta} = |M_{q\beta}|e^{i\phi_{q\beta}}$ in general; $\phi_{q\beta} = 0, \pi$ for Si, while $\phi_{q\beta} = \pm\pi/2$ for GaAs.

Next, discussion is made on how such difference of $M_{q\beta}$ affects the spectral profile of $\overline{A}_q(t_p;\omega_p)$ based on the PQ picture depicted in **Figure 2**. It is seen that there are two transition paths for the process: one is a direct path mediated by an optical transition matrix $D^{(r)}_{q\alpha_2}$ from LO-phonon state α_2 to the PQ ground state, and the other is a two-step resonant path mediated by $M_{q\beta}$ from α_2 to quasiboson state β, followed by a deexcited process mediated by an optical transition matrix $D^{(c)}_{q\alpha_2}$ from β to the PQ ground state. Accordingly, owing to Shore's model [62], the induced photoemission spectra in the proximity of $\omega_p \approx \omega^{(LO)}_q$ is read as

$$\overline{A}_q(t_p;\omega_p) \approx \mathcal{C}_{q\beta} + \frac{\mathcal{A}_{q\alpha_2}\left(\omega_p - \omega^{(LO)}_q\right) + \mathcal{B}_{q\alpha_2}\Gamma_{q\alpha_2}/2}{\left(\omega_p - \omega^{(LO)}_q\right)^2 + \left(\Gamma_{q\alpha_2}/2\right)^2}, \tag{28}$$

where a set of Shore's spectral parameters of $\mathcal{A}_{q\alpha_2}$, $\mathcal{B}_{q\alpha_2}$, and $\mathcal{C}_{q\beta}$ are provided by

$$\begin{cases} \mathcal{A}_{q\alpha_2} = 2|D^{(c)}_{q\beta}||D^{(r)}_{q\alpha_2}||M_{q\beta}|\cos\phi_{q\beta} \\ \mathcal{B}_{q\alpha_2} = -2|D^{(c)}_{q\beta}||D^{(r)}_{q\alpha_2}||M_{q\beta}|\sin\phi_{q\beta} + \left|D^{(r)}_{q\alpha_2}\right|^2|M_{q\beta}|^2/\left(\Gamma_{q\alpha_2}/2\right) \\ \mathcal{C}_{q\beta} = \left|D^{(c)}_{q\beta}\right|^2 \end{cases} \tag{29}$$

and the natural spectral width is represented by $\Gamma_{q\alpha_2} = 2\pi\rho_{q\alpha_2}|M_{q\alpha_2}|^2$; $\rho_{q\alpha_2}$ and $M_{q\alpha_2}$ are the density of state of quasiboson and the coupling matrix at $\mathcal{E}_{q\beta} = \omega^{(LO)}_q$, respectively. The associated Fano's q parameter is determined in terms of Shore's parameters as $q_{q\alpha_2}(t_p) = r_{q\alpha_2}(t_p) + \sigma_{q\alpha_2}(t_p)\sqrt{\left[r_{q\alpha_2}(t_p)\right]^2 + 1}$ with $r_{q\alpha_2}(t_p) = \mathcal{B}_{q\alpha_2}/\mathcal{A}_{q\alpha_2}$ and $\sigma_{q\alpha_2}(t_p) = \mathcal{A}_{q\alpha_2}/|\mathcal{A}_{q\alpha_2}|$.

An asymmetric spectral profile is exclusively determined by $\mathcal{A}_{\boldsymbol{q}\alpha_2}$. It is seen that $\mathcal{A}_{\boldsymbol{q}\alpha_2}(t_p)$ vanishes for $\phi_{\boldsymbol{q}\beta} = \pm\pi/2$ and $\overline{A}_{\boldsymbol{q}}(t_p;\omega_p)$ becomes of symmetric shape with $|q_{\boldsymbol{q}\alpha_2}(t_p)|$ infinite. The spectral profile of GaAs shown in **Figure 8(b)** corresponds to this case. For $\phi_{\boldsymbol{q}\beta} \neq \pm\pi/2$, both $\mathcal{A}_{\boldsymbol{q}\alpha_2}(t_p)$ and $\mathcal{B}_{\boldsymbol{q}\alpha_2}(t_p)$ are finite, and $\overline{A}_{\boldsymbol{q}}(t_p;\omega)$ becomes of asymmetric shape with $|q_{\boldsymbol{q}\alpha_2}(t_p)|$ finite. The spectral profile of Si shown in **Figure 7(b)** corresponds to this case, where $\phi_{\boldsymbol{q}\beta} \approx 0, \pi$. For **Figures 7(c)** and **8(c)**, since $D^{(c)}_{\boldsymbol{q}\overline{\alpha}}$ and $|M_{\boldsymbol{q}\beta}|$ become negligibly small, $\overline{A}_{\boldsymbol{q}}(t_p;\omega)$ is governed by the second term of the expression of $\mathcal{B}_{\boldsymbol{q}\alpha_2}(t_p)$, and this becomes symmetric with $\Gamma_{\boldsymbol{q}\alpha_2} \approx 0$. To conclude, the effective coupling $M_{\boldsymbol{q}\beta}$ around $\mathcal{E}_{\boldsymbol{q}\beta} \approx \omega^{(LO)}_{\boldsymbol{q}}$ plays the crucial role of the manifestation of TFR, and the asymmetry of profile is mostly determined by $\phi_{\boldsymbol{q}\beta}$ as long as $|M_{\boldsymbol{q}\beta}|$ is still large.

Finally, the manifestation of TFR of Si is discussed from the viewpoint of the allocation of time constants $T_{\boldsymbol{q}12}$ and T_{12}, where one sets $T_{\boldsymbol{q}12} < T_{12}$. This is an important issue for deepening the understanding of TFR. As shown in Figure 7(b), in the region of $T_{\boldsymbol{q}12} \lesssim t_p < T_{12}$, the asymmetric spectral profile bursts into view from the structureless continuum $\tilde{\chi}_{\boldsymbol{q}}(t_p;\omega)$. Actually, in the early-time region of $t_p < T_{12}$, the excited carrier density is still populated enough around the energy region of $\mathcal{E}_{\boldsymbol{q}\beta} \approx \omega^{(LO)}_{\boldsymbol{q}}$ to couple strongly with LO-phonon, while the effect of $\tilde{\chi}_{\boldsymbol{q}}(t_p;\omega)$ is much suppressed in the region of $T_{\boldsymbol{q}12} \lesssim t_p$. As regards a different allocation of these time constants, for instance, $T_{\boldsymbol{q}12} \sim T_{12}$, the TFR profile is no longer observed in the region of $t_p < T_{12}$, since this is covered with still dominant contributions from $\tilde{\chi}_{\boldsymbol{q}}(t_p;\omega)$, and the effect of $M_{\boldsymbol{q}\beta}$ becomes too small to cause TFR in the region of $t_p \approx T_{12}$. Therefore, the allocation of time constants such as $T_{\boldsymbol{q}12} < T_{12}$ is a necessary condition for realizing the TFR of Si in $\overline{A}_{\boldsymbol{q}}(t_p;\omega)$; otherwise this never appears.

4. Conclusion

Transient and optically nonlinear FR in condensed matter is examined here, which differs from conventional FR processes caused by a weak external perturbation in a stationary system. In particular, the following two FR processes are discussed: one is the DFR of Floquet exciton realized in semiconductor superlattices driven by a strong cw laser, and the other is the TFR accompanied by the CP generated by an ultrashort pulse laser in bulk crystals of undoped Si and undoped GaAs.

It is shown that the physical quantities relevant to the DFR spectra can be controlled by modulating F_{ac} and ω. In particular, the quantities as a function of F_{ac} take the extrema due to the ac-Zener coupling between the photon sidebands of μ_1 and μ_2, when F_{ac} is suitably adjusted to satisfy the DL condition. Further, the strong ω dependence is explained on the basis of the Autler-Townes effect forming the anticrossing between these two photon sidebands. It is remarked that the spectral width shown in **Figures 5** and **6** seems too small to be confirmed by experiments. Actually, in the present calculations, the Coulomb many-body effect is neglected. At least at the Hartree-Fock level, the vertex correction to the Rabi energy would make the net ac-Zener coupling stronger to result in such a great DFR width that experimental measurement would be accessible.

As regards the TFR spectra, the PQ model succeeds in demonstrating the appearance of asymmetric spectral profile in Si in a flash, whereas the profile observed in GaAs remains symmetric; the obtained results are in harmony with the existing experimental ones [45]. The difference between Si and GaAs is attributed to the phase factor of the effective coupling $M_{q\beta}(t_p)$. To conclude, it is found that in order to realize the TFR in the CP dynamics, the following conditions are to be fulfilled simultaneously. First, the coupling of an LO-phonon with an electron-hole continuum is conducted by the LO-phonon deformation potential interaction rather than by the Fröhlich interaction. Second, photoexcited carriers are populated enough around the energy region $\mathcal{E}_{q\beta} \approx \omega_q^{(LO)}$ in the early-time region $T_{q12} < t_p < T_{12}$ with $T_{q12} \ll T_{12}$.

Acknowledgements

This work was supported by JSPS KAKENHI Grants No. JP21104504, JP23540360, and JP15K05121.

Author details

Ken-ichi Hino[1,2]*, Yohei Watanabe[3], Nobuya Maeshima[2] and Muneaki Hase[1]

*Address all correspondence to: hino@ims.tsukuba.ac.jp

1 Faculty of Pure and Applied Sciences, University of Tsukuba, Tsukuba, Japan

2 Center for Computational Science, University of Tsukuba, Tsukuba, Japan

3 Graduate School of Pure and Applied Sciences, University of Tsukuba, Tsukuba, Japan

References

[1] Fano U. Physics Review. 1961;**124**. DOI: 10.1103/PhysRev.124.1866

[2] Bohn JL, Julienne PS. Physical Review A. 1997;**56**. DOI: 10.1103/PhysRevA.56.1486

[3] Ciurylo R, Tiesinga E, Julienne PS. Physical Review A. 2006;**74**. DOI: 10.1103/PhysRevA.74.022710

[4] Enomoto K, Kasa K, Kitagawa M, Takahashi Y. Physical Review Letters. 2008;**101**. DOI: 10.1103/PhysRevLett.101.203201

[5] Kouchi K. Superexcited states of molecules. In: Hiraoka K, editor. Fundamentals of Mass Spectrometry. Berlin: Springer-Verlag; 2013. DOI: 10.1007/978-1-4614-7233-9. Chap. 5.

[6] Kobayashi K, Aikawa H, Katsumoto S, Iye Y. Physical Review Letters. 2002;**88**. DOI: 10.1103/PhysRevLett.88.256806

[7] Xu B, Dai YM, Zhao LX, Wang K, Yang R, Zhang W, Liu JY, Xiao H, Chen GF, Trugman SA, Zhu J-X, Taylor AJ, Yarotski DA, Prasankumar RP, Qiu XG. Nature Communications. 2017;**8**. DOI: 10.1038/ncomms14933

[8] Bar-Ad S, Kner P, Marquezini MV, Mukamel S, Chemla DS. Physical Review Letters. 1997;**78**. DOI: 10.1103/PhysRevLett.78.1363

[9] Hino K. Physical Review B. 2000;**62**. DOI: 10.1103/PhysRevB.62.R10626

[10] Hino K. Physical Review B. 2001;**64**. DOI: 10.1103/PhysRevB.64.075318

[11] Hino K, Toshima N. Physical Review B. 2005;**71**. DOI: 10.1103/PhysRevB.71.205326

[12] Chu S-I, Telnov DA. Physics Reports. 2004;**390**. DOI: 10.1016/j.physrep.2003.10.001

[13] Potvliege RM, Shakeshaft R. In: Gavrila M, editor. Atoms in Intense Laser Fields. New York: Academic Press; 1992. p. 373

[14] Kroner M, Govorov AO, Remi S, Biedermann B, Seidl S, Badolato A, Petroff PM, Zhang W, Barbour R, Gerardot BD, Warburton RJ, Karrai K. Nature. 2008;**451**. DOI: 10.1038/nature06506

[15] Maeshima N, Hino K. Physical Review B. 2012;**85**. DOI: 10.1103/PhysRevB.85.205305

[16] Maeshima N, Yamada K, Hino K. Journal of Physics: Condensed Matter. 2013;**25**. DOI: 10.1088/0953-8984/25/43/435801

[17] Russell JP. Applied Physics Letters. 1965;**6**:223. DOI: 10.1063/1.1754144

[18] Parker JH Jr, Feldman DW, Ashkin M. Physics Review. 1967;**155**. DOI: 10.1103/PhysRev.155.712

[19] Hart TR, Aggarwal RL, Lax B. Physical Review B. 1970;**1**. DOI: 10.1103/PhysRevB.1.638

[20] Cerdeira F, Cardona M. Physical Review B. 1972;**5**. DOI: 10.1103/PhysRevB.5.1440

[21] Belitsky VI, Cantarero A, Cardona M, Trallero-Giner C, Pavlov ST. Journal of Physics: Condensed Matter. 1997;**9**. DOI: 10.1088/0953-8984/9/27/022

[22] Jin K-J, Zhang J, Chen Z-H, Yang G-Z, Chen ZH, Shi XH, Shen SC. Physical Review B. 2001;**64**. DOI: 10.1103/PhysRevB.64.205203

[23] Fano U, Rau ARP. Atomic Collisions and Spectra. Orlando: Academic Press, Inc; 1986 Chaps. 7–11

[24] Knight PL, Lauder MA, Dalton BJ. Physics Reports. 1990;**190**. DOI: 10.1016/0370-1573(90)90089-K

[25] Kukuu A, Amano T, Karasawa T, Maeshima N, Hino K. Physical Review B. 2010;**82**. DOI: 10.1103/PhysRevB.82.115315

[26] Nemoto Y, Hino K, Maeshima N. Physical Review B. 2013;**87**. DOI: 10.1103/PhysRevB.87.205305

[27] Meier T, Schulze A, Thomas P, Vaupel H. Physical Review B. 1995;**51**. DOI: 10.1103/PhysRevB.51.13977

[28] Siegner U, Mycek M-A, Glutsch S, Chemla DS. Physical Review Letters. 1995;**74**. DOI: 10.1103/PhysRevLett.74.470

[29] Siegner U, Mycek M-A, Glutsch S, Chemla DS. Physical Review B. 1995;**51**. DOI: 10.1103/PhysRevB.51.4953

[30] Hino K, Goto K, Toshima N. Physical Review B. 2004;**69**. DOI: 10.1103/PhysRevB.69.035322

[31] Watanabe Y, Hino K. M, Hase, and N. Maeshima. Physical Review B. 2017;**95**. DOI: 10.1103/PhysRevB.95.014301

[32] Bartal B, Kozma IZ, Stepanov AG, Almási G, Kuhl J, Riedle E, Hebling J. Applied Physics B: Lasers and Optics. 2007;**86**. DOI: 10.1007/s00340-006-2512-7

[33] Karpowicz N, Dai J, Lu X, Chen Y, Yamaguchi M, Zhang L, Zhang C, Price-Gallagher M, Fletcher C, Mamer O, Lesimple A, Johnson K. Applied Physics Letters. 2008;**92**. DOI: 10.1063/1.2828709

[34] Hirori H, Doi A, Blanchard F, Tanaka K. Applied Physics Letters. 2011;**98**. DOI: 10.1063/1.3560062

[35] Shirley J. Physics Review. 1965;**138**. DOI: 10.1103/PhysRev.138.B979

[36] Holthaus M. Physical Review Letters. 1992;**69**. DOI: 10.1103/PhysRevLett.69.351

[37] Grifoni M, Hänggi P. Physics Reports. 1998;**304**. DOI: 10.1016/S0370-1573(98)00022-2

[38] Dunlap DH, Kenkre VM. Physical Review B. 1986;**34**. DOI: 10.1103/PhysRevB.34.3625

[39] Keay BJ, Zeuner S, Allen SJ Jr.,Maranowski KD,Gossard AC, Bhattacharya U, and Rodwell MJW, Physical Review Letters **75**, (1995). DOI: 10.1103/PhysRevLett.75.4102

[40] Madison KW, Fischer MC, Diener RB, Niu Q, Raizen MG. Physical Review Letters. 1998;**81**. DOI: 10.1103/PhysRevLett.81.5093

[41] Eckardt A, Holthaus M, Lignier H, Al Z, Ciampini D, Morsch O, Arimondo E. Physical Review A. 2009;**79**. DOI: 10.1103/PhysRevA.79.013611

[42] Longhi S, Marangomi M, Lobino M, Ramponi R, Laporta P, Cianci E, Foglietti V. Physical Review Letters. 2006;**96**. DOI: 10.1103/PhysRevLett.96.243901

[43] Della Valle G, Ornigotti M, Cianci E, Foglietti V, Laporta P, Longhi S. Physical Review Letters. 2007;**98**. DOI: 10.1103/PhysRevLett.98.263601

[44] Szameit A, Garanovich IL, Heinrich M, Sukhorukov AA, Dreisow F, Pertsch T, Nolte S, Tünnermann A, Longhi S, Kivshar YS. Physical Review Letters. 2010;**104**. DOI: 10.1103/PhysRevLett.104.223903

[45] Hase M, Kitajima M, Constantinescu AM, Petek H. Nature (London). 2003;**426**:51. DOI: 10.1038/nature02044

[46] Gaal P, Kuehn W, Reimann K, Woerner M, Elsaesser T, Hey R. Nature. 2007;**450**. DOI: 10.1038/nature06399

[47] Hase M, Ishioka K, Demsar J, Ushida K, Kitajima M. Physical Review B. 2005;**71**. DOI: 10.1103/PhysRevB.71.184301

[48] Misochko OV, Lebedeva MV. JETP **120**; 2015. DOI: 10.1134/S1063776115020168

[49] Misochko OV. JETP. 2001;**92**. DOI: 10.1134/1.1354682

[50] Kato K, Ishizawa A, Oguri K, Tateno K, Tawara T, Gotoh H, Kitajima M, Nakano H. Japanese Journal of Applied Physics. 2009;**48**. DOI: 10.1143/JJAP.48.100205

[51] Lee JD, Inoue J, Hase M. Physical Review Letters. 2006;**97**. DOI: 10.1103/PhysRevLett.97.157405

[52] Mahan GD. Many-Particle Physics. New York: Plenum; 1981. DOI: 10.1007/978-1-4757-5714-9. Chaps. 4 and 5.

[53] Riffe DM. Physical Review B. 2011;**84**. DOI: 10.1103/PhysRevB.84.064308

[54] Hino K, Tong XM, Toshima N. Physical Review B. 2008;**77**. DOI: 10.1103/PhysRevB.77.045322

[55] Maeshima N, Hino K. Computer Physics Communications. 2012;**183**. DOI: 10.1016/j.cpc.2011.07.022

[56] Glutsch S, Bechstedt F. Physical Review B. 1999;**60**. DOI: 10.1103/PhysRevB.60.16584

[57] Meystre P, Sargent M III. Elements of Quantum Optics. 3rd ed. Berlin: Springer-Verlarg; 1999. DOI: 10.1007/978-3-540-74211-1. Chaps. 3 and 15

[58] Morse PM, Feshbach H. Methods of Theoretical Physics. New York: McGraw-Hill; 1953 Chap. 7

[59] Schäfer W, Wegener M. Semiconductor Optics and Transport Phenomena. Berlin: Springer-Verlag; 2002. DOI: 10.1007/978-3-662-04663-0. Chaps. 2, 10, and 11.

[60] Fetter AL, Walecka JD. Quantum Theory of Many-Particle Systems. New York: McGraw-Hill, Inc.; 1971 Chaps. 3–5

[61] Yu PY, Cardona M. Fundamentals of Semiconductors. 4th ed. Berlin: Springer-Verlarg; 2010. DOI: 10.1007/978-3-642-00710-1. Chaps. 3 and 7

[62] Shore BW. Reviews of Modern Physics. 1967;**39**. DOI: 10.1103/RevModPhys.39.439